International Journal of Hydrogen Energy. 42 (10): pp. 7246-7251, 2017.

A $La_{0.8}Sr_{0.2}MnO_3/La_{0.6}Sr_{0.4}Co_{0.2}Fe_{0.8}O_{3-\delta}$ core-shell structured cathode by a rapid sintering process for solid oxide fuel cells

Na Ai, Kongfa Chen, San Ping Jiang*

Fuels and Energy Technology Institute & Department of Chemical Engineering, Curtin University, Perth, WA 6102, Australia

Abstract

A $La_{0.8}Sr_{0.2}MnO_3$ (LSM)/$La_{0.6}Sr_{0.4}Co_{0.2}Fe_{0.8}O_{3-\delta}$ (LSCF) core-shell structured composite cathode of solid oxide fuel cells (SOFCs) has been fabricated by wet infiltration followed by a rapid sintering (RS) process. The RS is carried out by placing LSCF infiltrated LSM electrodes directly into a preheated furnace at 800°C for 10 min and cooling down very quickly. The heating and cooling step takes about 20 s, substantially shorter than 10 h in the case of conventional sintering (CS) process. The results indicate the formation of a continuous and almost non-porous LSCF thin film on the LSM scaffold, forming a LSCF/LSM core-shell structure. Such RS-formed infiltrated LSCF-LSM cathodes show an electrode polarization resistance of 2.1 Ω cm^2 at 700°C, substantially smaller than 88.2 Ω cm^2 of pristine LSM electrode. The core-shell structured LSCF-LSM electrodes also show good operating stability at 700°C and 600°C over 24-40 h.

Keywords: Solid oxide fuel cells; infiltration; rapid sintering process; core-shell structure; LSCF; LSM cathode.

* Corresponding author. Tel.: +61 8 9266 9804; fax: +61 8 9266 1138.
Email addresses: s.jiang@curtin.edu.au (S.P. Jiang)

1. Introduction

Solid oxide fuel cells (SOFCs) are an electrochemical device to directly convert chemical energy of fuels to electrical energy with high efficiency and low emissions. Nanostructured electrodes with nanoparticles supported on rigid scaffold have been paid with great attention for their potential application in intermediate temperature SOFCs at 600-800 ^{o}C. The catalytically active nanoparticles with special structures such as core-shell structures commonly employed in the development of highly active electrocatalysts for low temperature protonic exchange membrane fuel cells (PEMFCs) [1, 2] could dramatically enhance the electrochemical performance and stability of the electrodes of SOFCs. Thus core-shell like nanostructures have been developed in order to enhance the electrochemical activity and stability of the electrodes of SOFCs [3-7]. Liu *et al* [8, 9] prepared a core-shell structured cathode by infiltrating a dense (La,Sr)MnO_3 (LSM) thin film into $La_{0.6}Sr_{0.4}Co_{0.2}Fe_{0.8}O_3$ (LSCF) scaffold, which significantly enhanced the operating durability and performance of LSCF electrodes at 850^{o}C for ~600 h. Zhou *et al* [10] fabricated a dense La_2NiO_4 (LN) thin layer in BSCF scaffold by infiltration followed by a microwave treatment; the LN shell substantially increased the stability of BSCF in 10% CO_2 at 600^{o}C. Kim *et al* [11] coated a Pd core by CeO_2 shell via self-assembly method, and found that the Pd/CeO_2 core/shell nanoparticles in the (La,Sr)(Cr,Mn)O_3 (LSCM)/YSZ scaffold had a much better thermal stability than the infiltrated Pd nanoparticles.

As shown above solution infiltration/impregnation is one of the most common, simplest approaches to prepare nanostructured electrodes. However, the morphology, size and distribution of nanoparticles are significantly affected by parameters such as wetting property, dispersant, heating rate, and heat-treatment temperature [12-16]. Unlike the counterpart in low temperature PEMFCs, one significant challenge for fabrication of core-shell structures

for SOFCs is the significant grain growth and agglomeration of the electrodes associated with the sintering and long duration at high temperature (800-1100^{o}C). Thus, the reduction in the duration during the heating and cooling steps of the conventional sintering (CS) should substantially reduce the agglomeration of the infiltrated nanoparticles, resulting in the formation of core-shell nanostructure. To demonstrate the concept, we apply a rapid sintering (RS) process for LSCF infiltrated LSM electrodes by substantial increase of the heating rate by directly placing the infiltrated samples to the pre-heated furnace. The RS process bypasses the slow heating and cooling stage of CS process, thus can effectively reduce the agglomeration of infiltrated LSCF nanoparticles on LSM scaffold, forming a core-shell like structure.

2. Experimental

Electrolyte pellets of ~0.8 mm in thickness and 18 mm in diameter were fabricated by die pressing 8 mol% Y_2O_3-stabilized ZrO_2 (YSZ, Tosoh) and sintering at 1500^{o}C for 4 h. $La_{0.8}Sr_{0.2}MnO_3$ (LSM, Fuel Cell Materials) slurry was applied on YSZ by slurry coating and sintered at 1100 ^{o}C for 2 h to form 3-6 μm thick LSM electrodes. Dense LSM bar samples were also prepared by die pressing and sintered at 1350^{o}C for 5 h. Use of bar sample favors the observation of microstructure after the surface modification by infiltration.

$La_{0.6}Sr_{0.4}Co_{0.2}Fe_{0.8}(NO_3)_x$ solution of 0.0625 mol L^{-1} was prepared by dissolving $La(NO_3)\cdot 6H_2O$ (99.9%, Alfa Aesar), $Sr(NO_3)_2$ (99.0%, Sigma Aldrich), $Co(NO_3)_2\cdot 6H_2O$ (98.0-102.0%, Alfa Aesar), $Fe(NO_3)_3\cdot 9H_2O$ (≥98%, Sigma-Aldrich) and citric acid in de-ionized water. 2% Triton X-100 (99.95%, Sigma-Aldrich) as dispersant and 2 mol% $LiNO_3$ (≥99.0%, Sigma-Aldrich) as sintering agent were added to the solution. The solution was infiltrated into porous electrodes as well as the bar samples of LSM. The infiltrated samples were then heat-treated by a rapid sintering or RS process. In this RS process, a quartz tube

furnace was pre-heat-treated to 800ºC, and the samples were then directly placed into the furnace in <5 seconds and hold for 10 min. LSCF infiltrated LSM electrode/bar samples were also heated with conventional sintering (CS) process by heating the sample to 800ºC with heating rate of 2ºC/min, hold for 120 min and cooling down to 500ºC with cooling rate of 2ºC/min, then naturally cooling to room temperature. The overall period for the RS and CS is about 11 min and 12h, respectively. Fig. 1 illustrates the schematic diagram of the rapid sintering process to form the core/shell structure, in comparison with the conventional sintering process.

The electrochemical activity and stability of the electrodes was measured by a Gamry Reference 3000 potentiostat. Impedance responses were measured under open circuit in a frequency range of 0.1 Hz-100 kHz and a signal amplitude of 10 mV. The electrode polarization resistance, R_E, was obtained from the differences between the high and low frequency intercepts, and electrode ohmic resistance, R_Ω was obtained from the high frequency intercept. The impedance behavior for the O_2 reduction was also studied as a function of cathodic current passage at 200 mA cm^{-2} and 600-700ºC. The current passage treatment was interrupted from time to time to measure the impedance curves. Scanning electron microscopy (SEM, Zeiss Neon 40EsB) was used to examine the microstructure of the samples. The phase of LSCF powder prepared by the rapid sintering process was confirmed by X-ray diffractometry (XRD, Bruker D8 Advance).

2. Results and discussion

Fig. 2 shows the SEM micrographs of surface of a pristine LSM and LSCF infiltrated LSM in the form of porous electrodes and dense bar samples. In the case of porous electrodes, the LSM structure is characterized by interconnected particles in the size range of 0.2-0.5 μm (Fig. 2a). For the infiltrated LSCF-LSM electrode prepared by RS process, dense thin LSCF

coating is observed to covers the entire surface of LSM grains in a very homogeneous manner (Fig. 2b). XRD pattern of LSCF powder prepared by the RS process shows typical cubic perovskite peaks, which indicates the successful synthesis of LSCF crystal phase (Fig.2h).

For the bar samples, LSM is well sintered with a grain size in the range of 8-25 μm, and there are distinct crystal facets on the grain surface (Fig. 2c). The CS of the LSCF infiltrated LSM results in formation of a porous LSCF film comprising of nanoparticles in the size range of 50 nm (Fig. 2d); while for the RS process, a uniform and crack-free dense LSCF thin film is formed on the LSM surface, and the original crystal facets on the LSM grains are no longer observable (Fig. 2e). The morphology of the dense LSCF film is also retained after heat-treatment at 700°C in air for 100 h (Fig. 2f). In the case of an infiltrated LSCF-LSM electrode with RS, the dense thin film is maintained after the cathodic current passage at 200 mA cm^{-2} and 600°C for 40 h (Fig.2g), demonstrating the excellent thermal stability of the core-shell structure. This is consistent with the high thermal stability of LSCF infiltrated LSM bar samples heat-treated at 700°C for 100 h (Fig. 2). The results demonstrate the superior thermal stability of dense thin film over the easily agglomerated nanoparticles [17].

Fig. 3 is the IR free-electrode overpotential curves and impedance responses of pristine LSM and infiltrated LSCF-LSM electrodes at 700°C. The cathodic overpotential (η_c) of LSM electrode is substantially reduced by the LSCF infiltration (Fig. 3a). η_c of the LSM electrode increases rapidly with the increase of current, reaching 0.59 V at a cathodic current of 0.05 A cm^{-2}, followed by a gradual increase to 0.71 V at a cathodic current of 0.20 A cm^{-2}. On the other hand, η_c of the infiltrated LSCF-LSM electrode increases much more slowly. At a cathodic current of 0.05 and 0.20 A cm^{-2}, η_c is 0.086 and 0.21 V, respectively, substantially smaller than 0.59 and 0.71 V of the LSM electrodes. The impedance responses of LSM electrode are characterized by a large depressed arc with an electrode polarization resistance

(R_E) of 88.2 Ω cm^2 (Fig. 3b). After the infiltration of the LSCF film, the electrode activity of LSM is significantly enhanced with a R_E of 2.1 Ω cm^2, a reduction by 41 times compared to that of the pristine LSM. The activity enhancement is particularly pronounced in the low frequency region, which indicates the promotion effect of LSCF infiltration on the oxygen dissociation/surface diffusion process of LSM electrode [18, 19]. The activation energy for the O_2 reduction reaction on the infiltrated LSCF-LSM is ~108 kJ mol^{-1}, identical to that of the pristine LSM (Fig.3c), indicating that the reaction mechanism on LSM is not affected by the LSCF infiltration. This indicates that the incorporated LSCF film most likely acts as an activity promoter.

Fig. 4 displays the electrode stability curves during the cathodic current passage at 200 mA cm^{-2}, 700ºC and 600ºC. η_c of the LSM electrode is activated by the polarization at 700ºC, as evident by the decrease of η_c from the initial 0.69 V to 0.37 V after polarized for 24 h (Fig. 4a). On the other hand, the magnitude of decrease of η_c is much less at a reduced temperature of 600ºC. The initial η_c is 1.0 V and is slightly reduced to 0.93 V after polarized for 40 h (Fig. 4b). Compared to the LSM electrodes, the infiltrated LSCF-LSM electrodes deliver a much smaller η_c during the polarization test. For the operating temperatures of 700 and 600ºC, η_c decreases rapidly in the first ~1 h, then increases slowly and eventually becomes more or less stable with further polarization. In the case of operating at 700ºC (Fig. 4a), the initial η_c before the polarization is 0.2 V, decreases to 0.05 V after polarized for 0.5 h and is stabilized at 0.12 V after 24 h. The η_c value after polarized for 24 h is even lower than the initial η_c. The performance activation of infiltrated LSCF-LSM electrodes in the first 1 h of polarization is different from that of LSM electrodes, though the reason is unclear at the present stage. Nevertheless, the enhanced electrode activity after the polarization indicates excellent electrode stability of the infiltrated LSCF-LSM electrodes under SOFC operating conditions.

The significant promotion of electrode activity of infiltrated LSCF-LSM electrodes is

attributed to the excellent oxygen surface exchange properties and high ionic conductivity of LSCF as well as the unique core/shell structure. The pristine LSM cathode is a predominantly electronic conductor with a negligible ionic conductivity e.g. 5.9×10^{-7} S cm^{-1} at 900ºC [20], and therefore the oxygen reduction reaction is limited at the electrode/electrolyte interface [21]. By contrast, LSCF is a mixed ionic and electronic conductor (MIEC) with an ionic conductivity of 8×10^{-3} S cm^{-1} and an electronic conductivity of ~300 S cm^{-1} at 800ºC [22]. It also has high oxygen surface exchange coefficient (k) of 1×10^{-4} cm S^{-1} and self-diffusion coefficient (D^*) of 5×10^{-6} cm^2 S^{-1} at 800 ºC [23], much higher than k=5.62×10^{-9} cm S^{-1} and D^*=4.0×10^{-15} cm^2 S^{-1} of LSM [24]. Therefore, the high degree coverage of a highly active LSCF thin film on LSM grains not only enhances the oxygen surface exchange properties by providing a high surface area, but also enlarges the active reaction sites from the electrode/electrolyte interface into the bulk of electrodes due to formation of a connected ionic conducting network. These factors contribute to the substantially enhanced dissociation and surface diffusion processes related to the low frequency electrode process (Fig. 3b).

3. Conclusions

As a proof of concept, a core-shell nanostructured LSCF infiltrated LSM cathode was successfully fabricated by a substantially decrease the sintering time at high temperatures, i.e., RS process. The instant ramping process bypasses the particle growth and agglomeration associated with slow heating and sintering process, and thus the original morphology of the shell by wet impregnation could be maintained. The RS approach is effective to prepare a dense thin shell at high temperatures. The dense LSCF thin film significantly enhances the electrode electrocatalytic activity of LSM for the O_2 reduction reaction. The infiltrated LSCF-LSM electrode reaches a R_E of 2.1 Ω cm^2 at 700ºC, respectively, a reduction by 41 times compared to 88.2 Ω cm^2 of the pristine LSM electrode. The activity enhancement is due to the significant increase of electrode ionic conductivity and enlargement of active surface

reaction site, leading to enhanced oxygen dissociation and surface diffusion processes for the O_2 reduction reaction on the LSM electrodes. Also, the formed shell shows the high thermal stability under the SOFC operation conditions.

Acknowledgements

The project is supported by Curtin University Research Fellowships and Australian Research Council under Discovery Project scheme (project number: DP150102025 & DP150102044), Australia. The authors acknowledge the facilities, scientific and technical assistance of the Curtin University Electron Microscope Facility and Curtin X-Ray Laboratory, both of which are partially funded by the University, State and Commonwealth Governments.

References

[1] Strasser P, Koh S, Anniyev T, Greeley J, More K, Yu C, et al. Lattice-strain control of the activity in dealloyed core–shell fuel cell catalysts. Nat Chem 2010;2:454-60.
[2] Cheng Y, Shen PK, Saunders M, Jiang SP. Core-Shell Structured PtRuCox Nanoparticles on Carbon Nanotubes as Highly Active and Durable Electrocatalysts for Direct Methanol Fuel Cells. Electrochim Acta 2015;177:217-26.
[3] Zhou W, Liang F, Shao Z, Chen J, Zhu Z. Heterostructured electrode with concentration gradient shell for highly efficient oxygen reduction at low temperature. Sci Rep 2011;1.
[4] Lee D, Jung I, Lee SO, Hyun SH, Jang JH, Moon J. Durable high-performance Sm0.5Sr0.5CoO3-Sm0.2Ce0.8O1.9 core-shell type composite cathodes for low temperature solid oxide fuel cells. International Journal of Hydrogen Energy 2011;36:6875-81.
[5] Lee S, Song HS, Hyun SH, Kim J, Moon J. LSCF-SDC core-shell high-performance durable composite cathode. Journal of Power Sources 2010;195:118-23.
[6] Su R, Lü Z, Jiang SP, Shen Y, Su W, Chen K. Ag decorated (Ba,Sr)(Co,Fe)O3 cathodes for solid oxide fuel cells prepared by electroless silver deposition. International Journal of Hydrogen Energy 2013;38:2413-20.
[7] Ai N, Chen K, Jiang SP, Lü Z, Su W. Vacuum-assisted electroless copper plating on Ni/(Sm,Ce)O2 anodes for intermediate temperature solid oxide fuel cells. International Journal of Hydrogen Energy 2011;36:7661-9.
[8] Lynch ME, Yang L, Qin WT, Choi JJ, Liu MF, Blinn K, et al. Enhancement of La0.6Sr0.4Co0.2Fe0.8O3-δ durability and surface electrocatalytic activity by La0.85Sr0.15MnO3±δ investigated using a new test electrode platform Energy & Environmental Science 2011;4:2249-58.

[9] Ding D, Li X, Lai SY, Gerdes K, Liu M. Enhancing SOFC cathode performance by surface modification through infiltration. Energy and Environmental Science 2014;7:552-75.
[10] Zhou W, Liang FL, Shao ZP, Zhu ZH. Hierarchical CO2-protective shell for highly efficient oxygen reduction reaction. Scientific Reports 2012;2.
[11] Kim J-S, Wieder NL, Abraham AJ, Cargnello M, Fornasiero P, Gorte RJ, et al. Highly Active and Thermally Stable Core-Shell Catalysts for Solid Oxide Fuel Cells. Journal of The Electrochemical Society 2011;158:B596-B600.
[12] Sholklapper TZ, Lu C, Jacobson CP, Visco SJ, De Jonghe LC. LSM-infiltrated solid oxide fuel cell cathodes. Electrochem Solid State Lett 2006;9:A376-A8.
[13] Zhao F, Wang ZY, Liu MF, Zhang L, Xia CR, Chen FL. Novel nano-network cathodes for solid oxide fuel cells. J Power Sources 2008;185:13-8.
[14] Lou XY, Liu Z, Wang SZ, Xiu YH, Wong CP, Liu ML. Controlling the morphology and uniformity of a catalyst-infiltrated cathode for solid oxide fuel cells by tuning wetting property. J Power Sources 2010;195:419-24.
[15] Vohs JM, Gorte RJ. High-Performance SOFC Cathodes Prepared by Infiltration. Adv Mater 2009;21:943-56.
[16] Burye TE, Nicholas JD. Precursor solution additives improve desiccated La0.6Sr0.4Co0.8Fe0.2O3–x infiltrated solid oxide fuel cell cathode performance. J Power Sources 2016;301:287-98.
[17] Shah M, Voorhees PW, Barnett SA. Time-dependent performance changes in LSCF-infiltrated SOFC cathodes: The role of nano-particle coarsening. Solid State Ionics 2011;187:64-7.
[18] Jiang SP, Zhang JP, Foger K. Deposition of chromium species at Sr-doped LaMnO3 electrodes in solid oxide fuel cells - II. Effect on O-2 reduction reaction. J Electrochem Soc 2000;147:3195-205.
[19] Jiang SP. A comparison of O-2 reduction reactions on porous (La,Sr)MnO3 and (La,Sr)(Co,Fe)O-3 electrodes. Solid State Ionics 2002;146:1-22.
[20] Yasuda I, Ogasawara K, Hishinuma M, Kawada T, Dokiya M. Oxygen tracer diffusion coefficient of (La, Sr)MnO3 ± δ. Solid State Ionics 1996;86–88, Part 2:1197-201.
[21] Lynch ME, Ding D, Harris WM, Lombardo JJ, Nelson GJ, Chiu WKS, et al. Flexible multiphysics simulation of porous electrodes: Conformal to 3D reconstructed microstructures. Nano Energy 2013;2:105-15.
[22] Ullmann H, Trofimenko N, Tietz F, Stover D, Ahmad-Khanlou A. Correlation between thermal expansion and oxide ion transport in mixed conducting perovskite-type oxides for SOFC cathodes. Solid State Ionics 2000;138:79-90.
[23] Li Y, Gerdes K, Horita T, Liu X. Surface Exchange and Bulk Diffusivity of LSCF as SOFC Cathode: Electrical Conductivity Relaxation and Isotope Exchange Characterizations. Journal of the Electrochemical Society 2013;160:F343-F50.
[24] De Souza RA, Kilner JA, Walker JF. A SIMS study of oxygen tracer diffusion and surface exchange in La0.8Sr0.2MnO3+[delta]. Materials Letters 2000;43:43-52.

Figure captions:

1. Schematic diagram of fabrication process of the core/shell structure by a rapid sintering approach, in comparison with the conventional sintering process.
2. SEM micrographs of cross sections of (a) an as-prepared LSM electrode, (b) an as-prepared 0.05 mg cm^{-2} LSCF infiltrated LSM electrode prepared by the rapid sintering, and surface of (c) an as-prepared LSM bar sample, an as-prepared 0.012 mg cm^{-2} LSCF infiltrated LSM bar sample prepared by (d) the conventional sintering, (e) the rapid sintering, (f) the infiltrated LSCF-LSM bar prepared by rapid sintering, after heat-treated at 700^{o}C in air for 100 h, and (g) a LSCF infiltrated LSM electrode prepared by rapid sintering after the cathodic current passage at 200 mA cm^{-2} and 600^{o}C for 40 h. Activation plots of R_E of pristine LSM and LSCF infiltrated LSM electrodes as a function of temperature is shown in (h).
3. (a) IR-free overpotential and (b) impedance responses of a pristine LSM electrode and a LSCF infiltrated LSM electrode prepared by rapid sintering, measured at 700^{o}C. In (b), the numbers are frequency in Hz, and the inset shows the entire impedance responses of LSM electrode.
4. Electrode overpotential curves of a pristine LSM electrode and a LSCF infiltrated LSM electrode prepared by the rapid sintering process as a function of cathodic current passage time at 200 mA cm^{-2}, measured at (a) 700^{o}C and (b) 600^{o}C.

Figure 1.

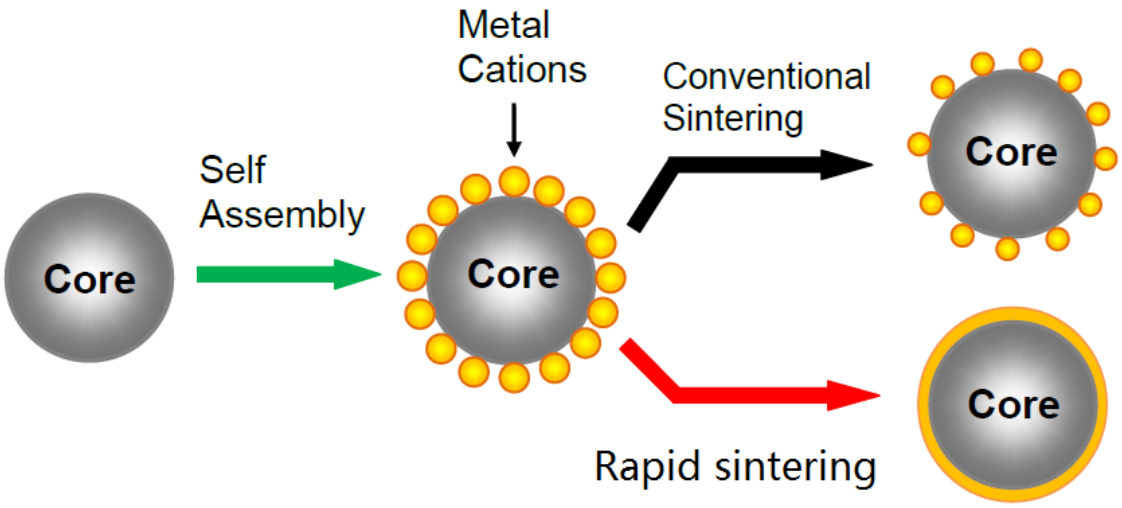
Metal
Cations
Conventional
Sintering
Core
Self
Assembly
Core
Core
Core
Rapid sintering

Figure 2.

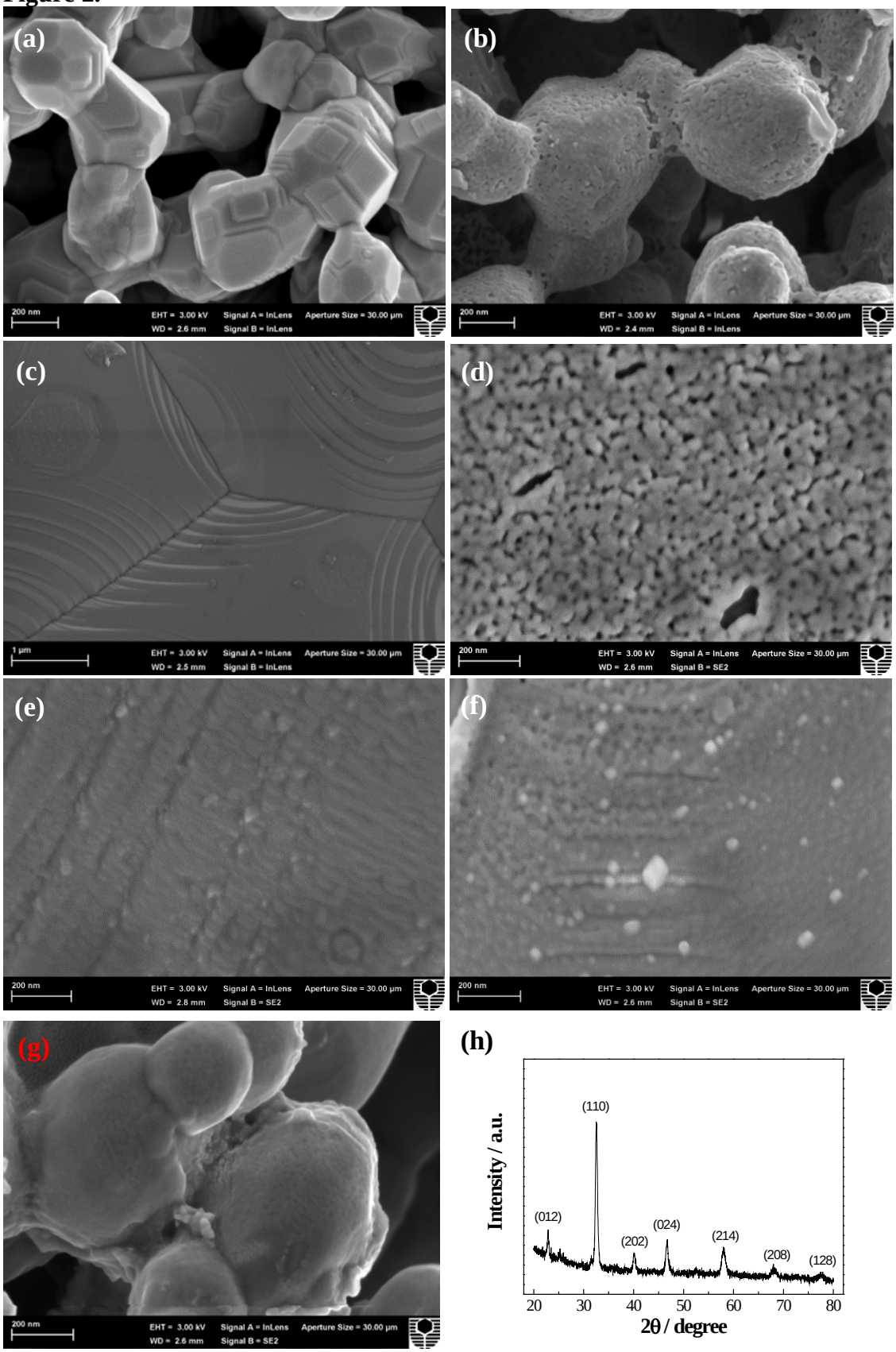
(a)
200 nm
EHT = 3.00 kV
WD = 2.6 mm
Signal A = InLens
Signal B = InLens
Aperture Size = 30.00 µm
(b)
200 nm
EHT = 3.00 kV
WD = 2.4 mm
Signal A = InLens
Signal B = InLens
Aperture Size = 30.00 µm
(c)
1 µm
EHT = 3.00 kV
WD = 2.5 mm
Signal A = InLens
Signal B = InLens
Aperture Size = 30.00 µm
(d)
200 nm
EHT = 3.00 kV
WD = 2.6 mm
Signal A = InLens
Signal B = SE2
Aperture Size = 30.00 µm
(e)
200 nm
EHT = 3.00 kV
WD = 2.8 mm
Signal A = InLens
Signal B = SE2
Aperture Size = 30.00 µm
(f)
200 nm
EHT = 3.00 kV
WD = 2.6 mm
Signal A = InLens
Signal B = SE2
Aperture Size = 30.00 µm
(g)
200 nm
EHT = 3.00 kV
WD = 2.6 mm
Signal A = InLens
Signal B = SE2
Aperture Size = 30.00 µm
(h)
Intensity / a.u.
(012)
(110)
(202)
(024)
(214)
(208)
(128)
20
30
40
50
60
70
80
2θ / degree

Figure 3.

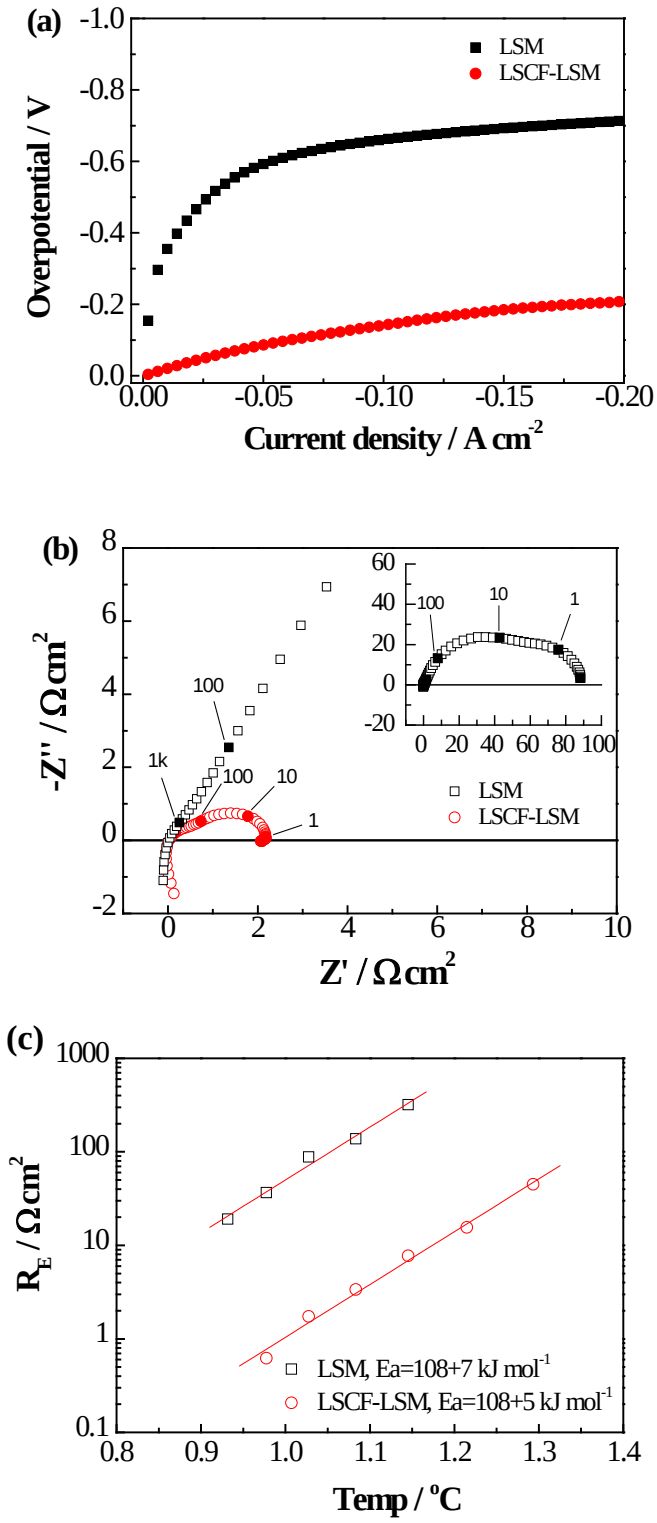
(a)
LSM
LSCF-LSM
Overpotential / V
Current density / A cm-2
(b)
-Z'' / Ωcm2
Z' / Ωcm2
100
1k
10
1
LSM
LSCF-LSM
(c)
RE / Ωcm2
Temp / °C
LSM, Ea=108+7 kJ mol-1
LSCF-LSM, Ea=108+5 kJ mol-1

Figure 4.

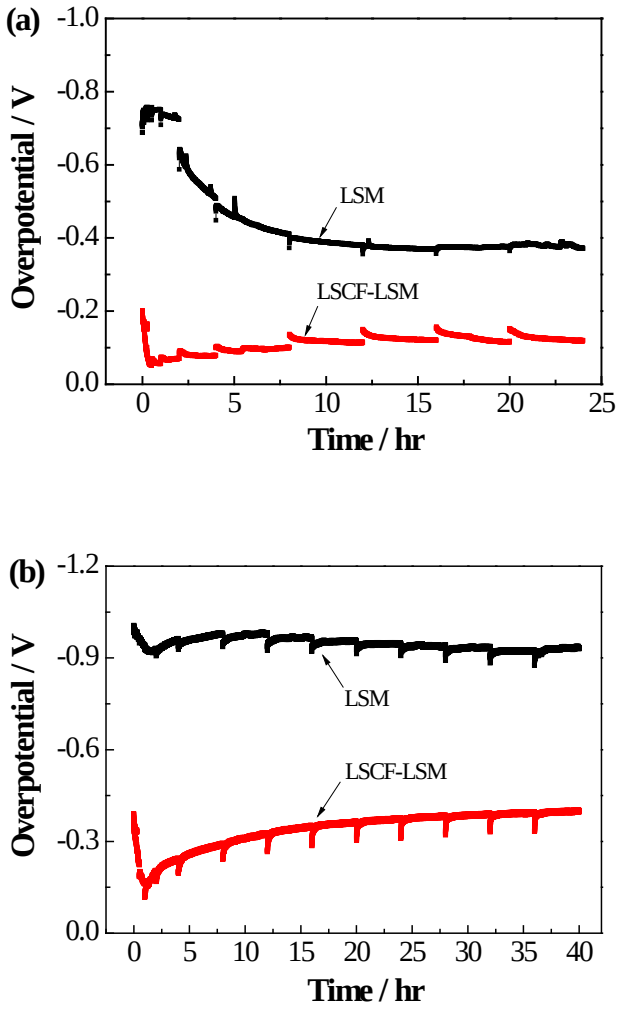
(a)
Overpotential / V
-1.0
-0.8
-0.6
-0.4
-0.2
0.0
LSM
LSCF-LSM
0
5
10
15
20
25
Time / hr
(b)
Overpotential / V
-1.2
-0.9
-0.6
-0.3
0.0
LSM
LSCF-LSM
0
5
10
15
20
25
30
35
40
Time / hr